Geochemistry, Geophysics, Geosystems®

RESEARCH ARTICLE
10.1029/2024GC011685

Ongoing Activity at Hunga Submarine Volcano, Tonga: The Case for Better Monitoring of Submarine Volcanoes Worldwide

Sharon L. Walker[1] **and Cornel E. J. de Ronde**[2]

[1]Pacific Marine Environmental Laboratory, National Oceanic and Atmospheric Administration, Seattle, WA, USA, [2]GNS Science, Lower Hutt, New Zealand

Abstract The powerful eruption of Hunga volcano (15-January-2022) excavated ~6.3 km^3 of pre-existing material, leaving behind an 855 m deep crater. The scientific and humanitarian response to this event was challenging due to the remote location, safety concerns, and COVID-19 pandemic restrictions. To investigate the status of ongoing eruptive/hydrothermal activity, this study used, for the first time, an un-crewed surface vessel operated remotely from >16,000 km away to make direct water column measurements within the crater and map its structure in detail. Intense turbidity and oxidation-reduction potential (ORP) anomalies located ongoing activity at sites on the steep inside crater slopes near both remaining islands. Mid-water acoustic reflectors indicated ongoing degassing, and positive ORP anomalies suggested gas composition was dominated by CO_2. At least 75% of the crater rim is shallower than 100 m, so any exchange with the surrounding ocean is limited by the depths of breaches in the rim (185 m between the islands and 290 m on the ENE side). This post-eruption bathymetry results in accumulation of emission products within the deep crater. There were no indications of the ongoing activity visible at the ocean surface, which highlights the limitations and inherent biases associated with relying on discolored surface water and/or atmospheric disturbances to determine eruption start/end dates at submarine volcanoes. This study demonstrates the value and need to add repeat hydrothermal plume and bathymetric surveys to our toolbox for monitoring submarine volcanoes, and the potential for un-crewed, remotely operated vessels to contribute significantly to these efforts.

Plain Language Summary The powerful eruption of Hunga volcano on 15-January-2022 sent a plume to space and generated unusual tsunamis. How the eruption impacted the submarine environment was more difficult to determine. We used a highly innovative, un-crewed vessel equipped with instruments to directly measure characteristics of the water within the 850 m deep crater excavated during the eruption and map the crater's shape in detail. These measurements showed there was ongoing hydrothermal/volcanic activity and CO_2 degassing within the crater 7 months after the eruption. The deepest parts of the crater are isolated from the surrounding ocean, so products of this activity become trapped within the crater. While the most powerful eruptions are rare, they can be quite hazardous. The results from this study emphasize the importance of monitoring submarine volcanoes long after signs of eruptions are no longer visible at the ocean surface or atmosphere. Operation of the un-crewed vessel >16,000 km from the study site was a major technological achievement and the first time that scientists could monitor operations in real time from anywhere around the globe. The success of this mission demonstrated the potential of this innovative technology to contribute to broader applications in ocean exploration, monitoring, and event response.

Key Points:

- Hydrothermal/volcanic activity and CO_2 degassing continued at Hunga volcano 7 months after the explosive 15 January 2022 eruption
- Turbidity and CO_2 are accumulating within the deep crater, which is isolated from the surrounding ocean deeper than ~200 m
- First use of a novel un-crewed vessel to conduct over-the-horizon bathymetric and water column surveys operated >16,000 km from the study site

Supporting Information:

Supporting Information may be found in the online version of this article.

Correspondence to:

S. L. Walker,
Sharon.L.Walker@noaa.gov

Citation:

Walker, S. L., & de Ronde, C. E. J. (2024). Ongoing activity at Hunga submarine volcano, Tonga: The case for better monitoring of submarine volcanoes worldwide. *Geochemistry, Geophysics, Geosystems*, *25*, e2024GC011685. https://doi.org/10.1029/2024GC011685

Received 4 JUN 2024
Accepted 11 JUL 2024

Author Contributions:

Conceptualization: Sharon L. Walker, Cornel E. J. de Ronde
Data curation: Sharon L. Walker
Formal analysis: Sharon L. Walker, Cornel E. J. de Ronde
Investigation: Sharon L. Walker, Cornel E. J. de Ronde
Methodology: Sharon L. Walker, Cornel E. J. de Ronde
Validation: Sharon L. Walker
Visualization: Sharon L. Walker

1. Introduction

The 15 January 2022 eruption of Hunga volcano, in the South Pacific island nation Kingdom of Tonga, was a powerfully explosive eruption (estimated magnitude = VEI ~ 6, Global Volcanism Program, 2022; Poli & Shapiro, 2022), that had global impacts and generated an ash plume that reached all the way to space (Proud et al., 2022). It was the first eruption of this magnitude to occur while a wide range of internationally supported Earth observing systems were in place and operational. These systems included numerous satellites, ocean and atmospheric monitoring stations, weather stations, tsunami warning systems, seismometers, tide gauges, ships at sea, and even human observations, which all rapidly provided a wealth of data about the impacts of the eruption on the atmosphere (e.g., Matoza et al., 2022; NASA, 2022; Zhu et al., 2022) and surface ocean (Barone et al., 2022). The eruption generated both local and widespread tsunamis (e.g., Kubota et al., 2022; Lynette et al., 2022) causing

Writing – original draft: Sharon L. Walker, Cornel E. J. de Ronde
Writing – review & editing: Sharon L. Walker, Cornel E. J. de Ronde

loss of life (at least 6 confirmed deaths: 4 in Tonga and 2 in Peru) and significant damage. An initial assessment of damage within Tonga due to ashfall and tsunamis was estimated at US$90.4 million (World Bank, 2022). Less destructive tsunamis generated by atmospheric Lamb waves (meteotsunamis) were detected globally (Carvajal et al., 2022; NOAA, 2022). The volcanic cone that had built up during the 2014–2015 eruption, connecting the once-separate islands of Hunga Tonga and Hunga Ha'apai (Garvin et al., 2018) and enlarged further when eruptions began again in December 2021, was completely removed by the 15 January 2022 climactic eruption, with the above-surface land mass of each island also significantly reduced (Global Volcanism Program, 2022).

It was more difficult to assess how the eruption impacted the seafloor or what the status of ongoing submarine volcanic and/or hydrothermal activity might be. Ships with the capabilities required for an event response are a limited resource. Rapid response cruises can be difficult to mobilize, especially for events in remote locations (Baker et al., 2012), and there are legitimate concerns for the safety of a fully staffed survey vessel sailing over the site of a shallow submarine eruption (e.g., Myojin-sho volcano, Nakano et al., 1954). Responding to the aftermath of this eruption, for both humanitarian assistance and scientific investigation of seafloor and environmental changes, was further complicated by restrictions in place at the time due to the COVID-19 pandemic. The first expedition that was organized to map the impact of the eruption on the seafloor set sail ∼2.5 months after the eruption but was forced to turn back when critical equipment was damaged *en route* (de Ronde, 2022). It was another month before the first relatively low-resolution map revealed the giant ∼850 m deep hole that the explosion left behind (Cronin and Tonga Geological Service, 2022; Stern, 2022).

There is ongoing debate as to whether the new deep hole in the seafloor is a caldera due to seafloor collapse after magma removal, an explosion crater, or was formed by a combination of mechanisms. By some definitions, the distinction between "caldera" and "crater" is merely one of size rather than process, so the terms have been used synonymously. However, the term "caldera" is more specifically used to identify a formation process related to magma withdrawal and structural subsidence (Lipman, 2000). We choose here to use the term "crater," as the more generic term, lacking proof of a definitive formation process related to subsidence for several reasons: the volume of existing material removed during the eruption (6.3 km^3 from the summit and 3.5 km^3 eroded from the flanks) accounts for nearly all the volume of new deposits on the seafloor identified by bathymetric differencing (Clare et al., 2023; Seabrook et al., 2023); the source (pre-existing or eruptive) and fate (proximal deposition or distal dispersion) of the estimated 1.9 km^3 in the atmospheric plume (Yuen et al., 2022) are unknown; there is significant uncertainty in volumes of magma erupted based on estimated changes to an inferred underlying magma chamber (Le Mevel et al., 2023); and the scalloped edges and lack of clear ring fault structures in the post-eruption morphology strongly suggests that the powerful explosion was dominantly responsible for the excavation of preexisting material (Henley et al., 2024), which can account for a major portion of the documented deposits.

During phase 1 of the NIWA-Nippon Foundation "Tonga Eruption Seabed Mapping Project" (TESMaP-1; April–May 2022) the R/V *Tangaroa* comprehensively mapped the seafloor surrounding Hunga volcano at 50 m resolution to a distance of 20 km, and to greater distances in select directions, but did not go directly over the summit's newly excavated crater due to safety concerns (Mackay, 2022; Seabrook et al., 2023; Williams et al., 2022). Sediment cores and seawater samples were also collected during this expedition, and a camera system provided seafloor observations to document regional environmental impacts (Mackay et al., 2022; Seabrook et al., 2023).

Here we present results from TESMaP phase 2 (TESMaP-2; July August 2022), which utilized the un-crewed surface vessel (USV) *Maxlimer* (SEA-KIT International; Figure S1 in Supporting Information S1) to investigate the status of ongoing hydrothermal or eruptive activity within the crater, map the distribution of subsurface plumes, and survey the bathymetry of the post-eruption edifice with 10 m resolution (Figure 1c; NIWA-Nippon Foundation, 2023).

This work is the first time that traditional plume-mapping methods, which combine vertical cast and tow-yo deployments of plume-tracing sensors, were attempted from an USV operated entirely in "over the horizon" mode from a command center >16,000 km away. The success of this mission demonstrates the utility and value of this major technological innovation, and establishes its potential for future application to ocean exploration, shallow submarine volcano monitoring, and event response missions.

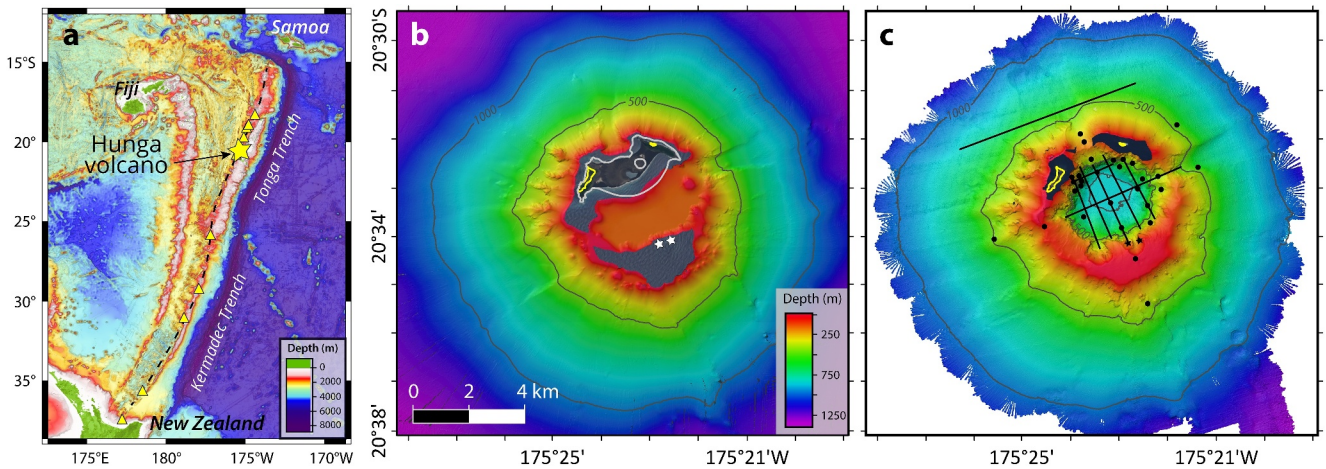

Figure 1. (a) Regional map showing location of Hunga volcano (yellow star) along the Tonga-Kermadec arc between New Zealand and Samoa (black dashed line). Small yellow triangles mark the locations of other arc volcanoes that have erupted since 2000 (see Table 1). (b) Pre-eruption (2016) bathymetry of Hunga volcano (Ferrini, 2022). Gray lines are 500 and 1,000 m depth contours. White polygons outline the extent of HT-HH island in early January 2022 and its crater lake. Yellow polygons outline the post-eruption islands. Gray polygons are areas that were too shallow for the ship to map at the time. (c) Post-eruption bathymetry of Hunga volcano acquired during TESMaP-2 from un-crewed surface vessel *Maxlimer* (NIWA-Nippon Foundation, 2023) showing the locations of vertical casts (black circles) and tow tracklines (thick black lines; see Figure S2 in Supporting Information S1 for greater detail). Gray lines are 500 and 1,000 m depth contours outside the crater, and 500 and 850 m depth contour inside the crater. Yellow polygons outline the post-eruption islands. Depth colors and scale bar for (c) are the same as shown in (b).

2. Geological Setting

Hunga volcano is one of about 80 submarine volcanoes that have formed along the ~2,550 km Tonga-Kermadec arc (Figure 1) where the Pacific plate subducts beneath the Australian plate at rates of 6–24 cm/yr (increasing from south to north; Smith & Price, 2006), and generates abundant seismic and volcanic activity. At least 8 arc volcanoes (both submarine and subaerial) are known to have erupted since 2000, several of them multiple times (Table 1, Figure 1a). Most of these volcanoes also had confirmed eruptions during the 20th century. Nearly all of these eruptions were confirmed and documented because of visually identifiable surface ocean or atmospheric indicators such as discolored water, pumice rafts, or ash and steam plumes that breached the surface or were injected higher into the atmosphere (Global Volcanism Program, 2024). About 80% of the submarine volcanoes along the Kermadec section of the arc are hydrothermally active (Arculus, 2006; Baker et al., 2003, 2019; de Ronde et al., 2001; Massoth et al., 2007), but their eruptive histories, especially for the deeper sites, are not well known.

The islands of Hunga Tonga and Hunga Ha'apai are the above sea-level portion of a conical edifice with a basal diameter of ~17 km at a depth of 1,200 m. The most recent major caldera-forming eruption is estimated to have occurred around 1100 CE (Brenna et al., 2022). Before the 15 January 2022 eruption, the maximum depth within the summit crater area was 155 m (Figure 1b; Ferrini, 2022). Comparison of pre- and post- eruption bathymetry grids revealed new scour channels along the outer flanks of the volcano and thick deposits from fast-moving turbidity currents as the eruption column collapsed into the ocean, sped across the seafloor and destroyed communications cables that the island nation relied on for connection with the rest of the world (Clare et al., 2023). However, there was no large-scale slope failure or mass wasting of the edifice (Seabrook et al., 2023). Structurally, the flanks of the edifice are essentially unchanged.

2.1. Post-Eruption Morphology Constrains Plume Distribution

The rim of the newly excavated crater (Figure 1c) has a diameter at the internal 200 m depth contour of ~3.5 km. Seventy five percent of the rim encircling the new crater is shallower than 100 m; 43% is shallower than 50 m, including the remaining islands that rise above sea level. A narrow breach (<1 km distance along the rim) with a maximum depth of 185 m is located on the north side between the two islands, while another breach on the ENE side is deeper than 200 m for a distance of ~800 m, with a maximum depth ~290 m. Thus, most of the rim is at or shallower than the thermocline, a proxy for the steep density gradient between the well-mixed surface layer and deeper ocean water masses. This geometry ensures that water within the 855 m deep crater is essentially isolated

Table 1
Confirmed Eruptions From Tonga-Kermadec Arc Volcanoes Since 2000

Arc section	Name	Location	Type	Month-year	1900–2000
Tonga	Volcano F	18.325°S, 174.365°W	Shallow submarine	September-2001	Unknown
				August-2019	
	Home Reef	18.992°S, 174.775°W	Ephemeral island	August-2006	Yes
				September-2022	
				October-2023	
	Late'iki (Metis Shoal)	19.18°S, 174.87°W	Ephemeral island	October-2019	Yes
	Tofua	19.75°S, 175.07°W	Subaerial	March-2004	Yes
				December-2021	
	Hunga	20.553°S, 175.384°W	Shallow submarine to subaerial	March-2009	Yes
				December 2014–January 2015	
				December 2021–January 2022	
	Volcano A	20.852°S, 175.55°W	Shallow submarine	2007	Yes
				January-2017	
Kermadec	Monowai	25.887°S, 177.188°W	Shallow submarine	May-2002	Yes
				November-2002	
				April-2003	
				March-2005	
				December-2006	
				February-2008	
				May-2009	
				May-2011	
				August-2012	
				January-2014	
				October-2014	
				November-2016 (no recent data)	
	Raoul Island	29.27°S, 177.92°W	Subaerial	March-2006	Yes
	Havre	31.08°S, 179.033°W	Deep submarine	July-2012	Unknown
	Rumble III	35.745°S, 178.478°E	Shallow submarine	July-2008	Yes
	Whakaari (White Island)	37.52°S, 177.18°E	Subaerial	March-2000	Yes
				February-2001	
				August-2012	
				April-2016	
				September-2016	
				December-2019	

Note. Eruption dates are from Global Volcanism Program (2024).

from the surrounding ocean deeper than ~200 m, resulting in a reduced density gradient within the crater and water mass properties that are similar to water outside the crater at this limiting depth (Figure 2; Staudigel et al., 2004; Walker and de Ronde, 2023).

Any exchange between the contents of the crater and open ocean are limited to the locations and depth ranges of the breaches, and are likely controlled by complex processes such as the interaction of ocean currents with the seamount, vertical displacement of isopycnals due to internal tides, or hydrothermal/volcanic venting with enough buoyancy to vertically transport plumes shallower than the rim depth (Staudigel et al., 2004). If lower-intensity hydrothermal and/or volcanic activity persists, the fluxes of heat, particles and chemicals can accumulate within the deep crater (S. Carey et al., 2013; Walker and de Ronde, 2023). Despite having only 300 m of wire on the USV *Maxlimer* winch (see Section 3.2), our survey provided valuable information about the locations

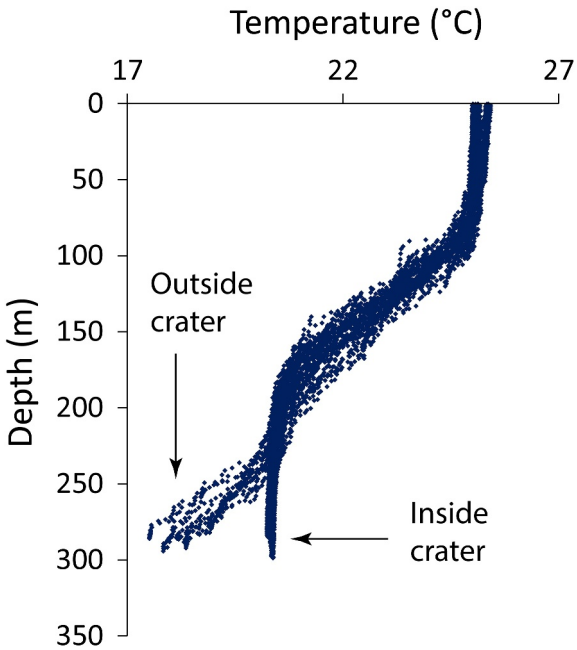

Figure 2. Temperature profiles from all vertical casts and tows showing water temperature within the crater is the same as external water at ~200–250 m depth, indicating that exchange with surrounding ocean water is controlled by the average depth at the ENE crater rim breach.

of ongoing venting and accumulation of hydrothermal and/or eruption products within the crater 6–7 months after the 15 January climactic eruption.

3. Methods

3.1. Remote Operations for a Safe Post-Eruption Survey

The Tonga Eruption Seabed Mapping Project phase 2 (TESMaP-2) utilized the USV *Maxlimer*, a 12 m X-class vessel owned and operated by SEA-KIT International. The vessel payload included a Kongsberg EM710 multibeam sonar system for bathymetric mapping and detecting midwater acoustic backscatter (or water column reflectors, WCR), and this smaller, lighter vessel was able to obtain high resolution multibeam data within the shallow areas that were inaccessible to the prior (2016) survey. Unlike autonomous vessels that have pre-programmed missions, USV *Maxlimer* was operated from SEA-KIT's Remote Operations Center in Tollesbury, Essex, UK, more than 16,000 km distant from the study site. Real-time operational control specifications and details are available from SEA-KIT (https://www.sea-kit.com). The seafloor mapping and water column (sensor) teams were located at their homes or offices in seven different countries around the world (UK, Ireland, Poland, Egypt, Australia, New Zealand, and USA). Real-time communications using WhatsApp® and web-based access to vessel status, weather conditions and other data were available to all participants 24 hr a day, which were essential for successful remote sensor deployments. Planning and operational up-date meetings included all participants and were held daily (virtually). Only two to three engineers were required to be present in Tonga to liaise with local officials, and manage physical logistics of the vessel and scientific payload (including vessel assembly, quality control, maintenance, and some data management tasks).

3.2. Plume Mapping

Direct water column measurements were made possible by the addition of an operator-controlled winch with 300 m of non-conducting cable and a custom-built cage that accommodated two Miniature Autonomous Plume Recorder (MAPR) instruments (Figure S1 in Supporting Information S1; Walker, 2023). MAPR sensors included temperature, pressure, turbidity (optical backscatter), and oxidation-reduction potential (ORP) to measure primary plume tracers (e.g., Baker et al., 2016 and references therein).

A total of 30 vertical casts and 8 tow-yo's (total distance traveled = 28 km) were completed between 27 July and 29 August 2022 both inside and outside the crater (Figure 1c and Figure S2 in Supporting Information S1), resulting in a spatially comprehensive survey of the hydrothermal and/or volcanic plumes in the water column. Optical backscatter (reported as dimensionless nephelometric turbidity units, or NTU) can be directly related to suspended particle concentration including, but not limited to, fine ash particles and hydrothermal precipitates, although the relationship is a function of particle size and composition (Baker et al., 2001). ORP is the measured electric potential between a platinum working electrode and an Ag/AgCl reference electrode (E, mV; Walker et al., 2007).

Absolute ORP values are subject to significant drift and hysteresis due to several factors (e.g., time required for electrodes to come to equilibrium with their environment, electrodes constantly moving through an environment that is not at equilibrium, and rapid response to reduced chemical species paired with slow "recovery" to pre-response values). As such, ORP anomalies (ΔE, mV) are qualitative indications of relative chemical differences between water masses, but have become reliable indictors of proximity to sources of hydrothermal venting and other seafloor settings where reduced chemical species are introduced into the water column (e.g., volcanic eruptions and methane seeps).

ORP responses can also qualitatively shed light on some aspects of the chemical composition of plumes. ORP values *decrease* rapidly in the presence of reduced chemical species, such as Fe^{2+}, H_2S, and H_2 that are out of

equilibrium with the surrounding seawater (Baker et al., 2016; Walker et al., 2007). Several factors contribute to the oxidation rate of these species, but Fe^{2+} and H_2, for example, are known to oxidize, or be biologically utilized, rapidly (e.g., Kadko et al., 1990; Statham et al., 2005), resulting in spatially limited ORP anomalies that indicate nearby sources. By contrast, ORP values *increase* in the presence of CO_2 but do not respond at all to CH_4 (Figure S3 in Supporting Information S1). It is important to note that the electrodes respond to the combined chemistry and reactivity of all redox species that may be present. In the majority of hydrothermal plumes, regardless of geological setting, ORP anomalies are negative, with Fe^{2+} or H_2S most likely dominating the signal. ORP anomalies with extremely rapidly decreasing voltages have been seen in plumes over submarine eruptions where very high concentrations of dissolved hydrogen were measured (Baker et al., 2011; Baumberger et al., 2014, 2020). Positive anomalies have been seen at a few locations where CO_2 could be attributed to dominating the response, for example, at Maug caldera in the Mariana arc where ΔCO_2 was enriched up to 119 μM, H_2S was not detected, and iron was nearly 100% in the particulate oxidized phase, even though total dissolvable iron concentrations were high (Figure S4 in Supporting Information S1; Resing et al., 2009). Positive ORP anomalies were also observed in areas of hydrothermal discharge in volcanic Lake Rotomahana (New Zealand) where CO_2 was strongly degassed (Mazot et al., 2014; Walker et al., 2016).

Negative anomalies are calculated as the difference between the value at the time voltages began a sustained decrease and the minimum value reached. To make direct comparisons of ORP profiles between casts with increasing ORP anomalies, ORP values were normalized to a constant surface value (arbitrarily chosen) and labeled E_n. Positive ORP anomalies were calculated as the difference between the maximum E_n value (which usually coincided with NTU_{max}) compared to the designated background cast where plume anomalies outside the crater were minimal (station 3–6; see Supporting Information S1 for further details).

Acoustic WCR are usually interpreted as gas bubbles because they are very efficient reflectors given the density difference between water and gas. WCR formed the basis for imaging the flux of CO_2 from NW Rota-1 while it was erupting in 2010 (Chadwick et al., 2014) and have been used to map methane seeps on continental margins (e.g., Merle et al., 2021). Real-time observations of midwater acoustic WCR from USV *Maxlimer* and preliminary locations of acoustic reflectors (later summarized by Ribo et al. (2023)) that could potentially indicate volcanic degassing at Hunga volcano helped guide our sampling locations.

4. Results

4.1. Plume Distributions Inside the Crater

Particle concentrations were elevated everywhere within the crater below ~125–150 m water depth, with average NTU_{max} ~ 0.8, an order-of-magnitude greater than the well-mixed surface layer (i.e., shallower than ~50 m) where NTU values were 0.08–0.09. The upper limit of the widespread particle plume within the crater coincided with the lower boundary of the thermocline, indicating emissions were generally not energetic enough to be transported vertically through the steeper density gradient to shallower depths at that time. A turbidity anomaly in the surface layer was seen at only one station offshore Hunga Ha'apai (station 1–10, $NTU_{max} = 0.17$ centered at 35 m, with no corresponding ORP anomaly) and may not have been directly related to active venting (e.g., particulates derived from erosion of the nearby island), although that station was where one of the most intense plume signals was observed from ~125 m to the deepest point of the cast (160 m).

Our survey was completed during 3 missions, with 11 days between the first and second missions, and 17 days between the second and third missions. During this time, there was no significant deepening of the top of the turbid layer that would suggest cessation of hydrothermal or eruptive input and subsequent settling of particles, removal by advection, or flushing of crater contents by intrusion and replacement with external water. Spatial differences in turbidity maxima were greater than temporal differences. This suggests that inputs at discrete locations generally balanced overall losses, which requires constant replenishment through ongoing venting during this 28-day timeframe.

Locations of ongoing venting were identified by intense particle plumes ($NTU_{max} > 1.0$) and ORP anomalies (ΔE to −70 mV) on the steep inside walls near both Hunga Tonga and Hunga Ha'apai islands (Figure 3). Each of these areas also had apparent WCR. The source of venting near Hunga Ha'apai was located ~500 m east of the island's shoreline at a depth of about 170–200 m, near the starting position for Tow-3 (Figure 3a and Figure S2 in Supporting Information S1). The sharply sloping seafloor (60°–70°) and proximity to the island made for

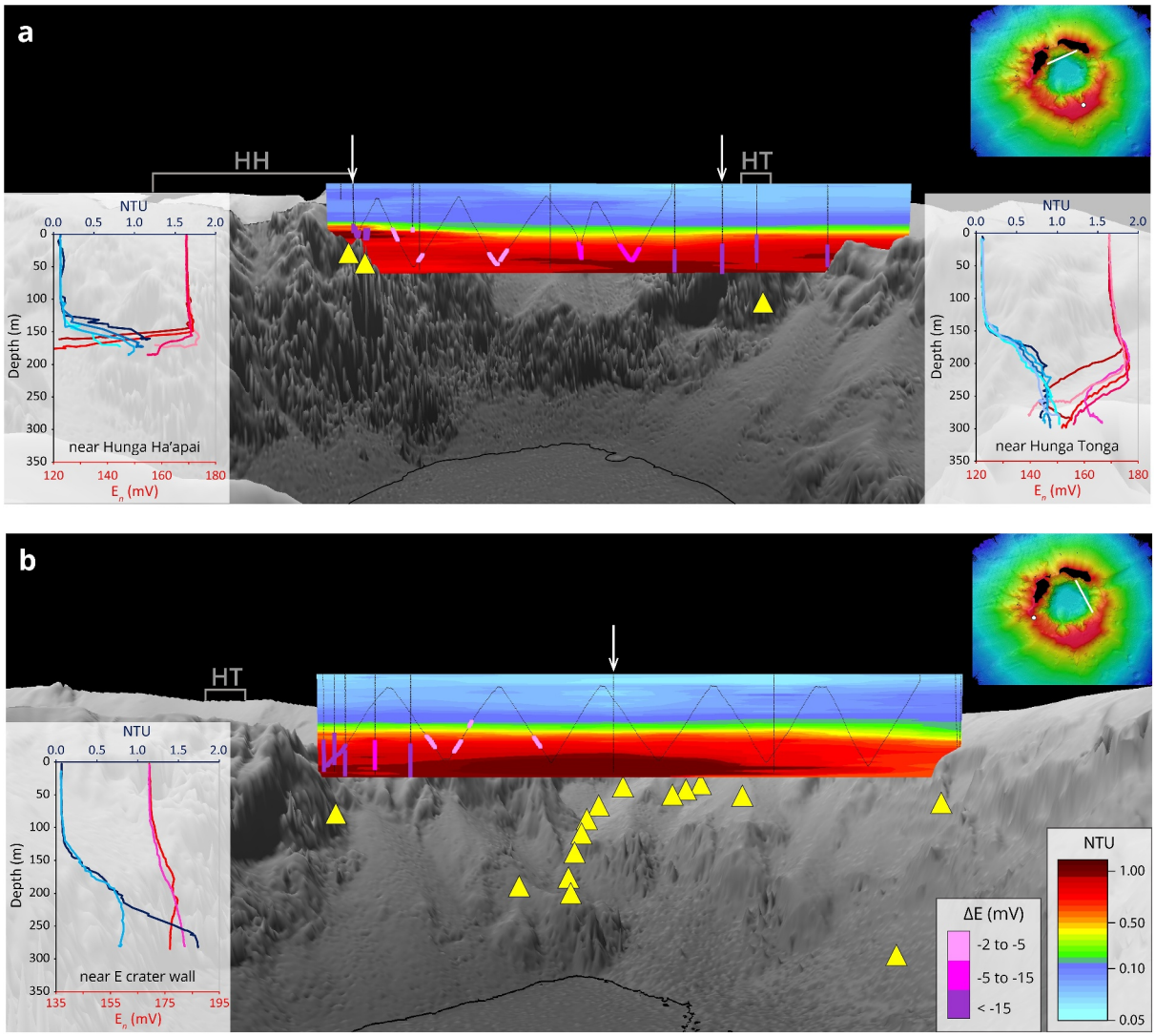

Figure 3. 3-d view of Hunga volcano crater particle plumes (NTU, color filled contour panels). Greyscale bathymetry is vertically exaggerated by a factor of 1.5. Negative oxidation-reduction potential (ORP) anomalies (ΔE, pink and purple lines) and data points (black dots) overlay the NTU contours. Map insets in the upper right corner of each panel show the location of the transects (white lines) and viewpoint (white dots) for each scene. Color scales for NTU and ΔE are the same for both panels and are shown in (b). Yellow triangles are preliminary locations of water column reflectors. Thin black line overlain on the greyscale bathymetry is the 850 m depth contour inside the crater. (a) Transect aligned with Tow 3 (see Figure S2 in Supporting Information S1) between the islands. White arrows show the locations of the NTU and normalized ORP profiles shown in the lower left and lower right corners, respectively. The locations of the islands are represented by gray lines and labels "HH" and "HT" for Hunga Ha'apai and Hunga Tonga, respectively. Lower left inset includes data from stations 1–10, 2–3, and the initial downcast from Tows 3 and 6 (see Figure S2 in Supporting Information S1). Lower right inset includes data from stations 1–7, 2–10, 2–11, 2–12, and the initial downcast for Tow 4. (b) Transect aligned with Tow 4 (see Figure S2 in Supporting Information S1) along the east side of the crater. White arrow shows the orientation of the NTU and ORP profiles shown in the lower left corner, which are aligned with the Tow 4 transect (dark blue, red) and the center of the crater (light blue, pink), respectively (stations 1–6 and 1–12). The location of Hunga Tonga is represented by the gray line labeled "HT" above the bathymetry.

challenging operating conditions since the instrument cage did not have an altimeter and we needed to rely on the multibeam (center beam) depth to determine how much wire could be safely payed out from the winch. This introduced uncertainty for the lower depth limits of the plume and altitude at the deepest point of the cast because depth under the instrument cage could change rapidly over the steep slope if the vessel position changed by mere meters (we prioritized safety for the vessel and equipment). However, turbidity and ORP anomaly distributions in vertical casts and portions of tows located within ~500 m of these stations were consistent with a 170–200 m depth range for the source(s) of venting in this area.

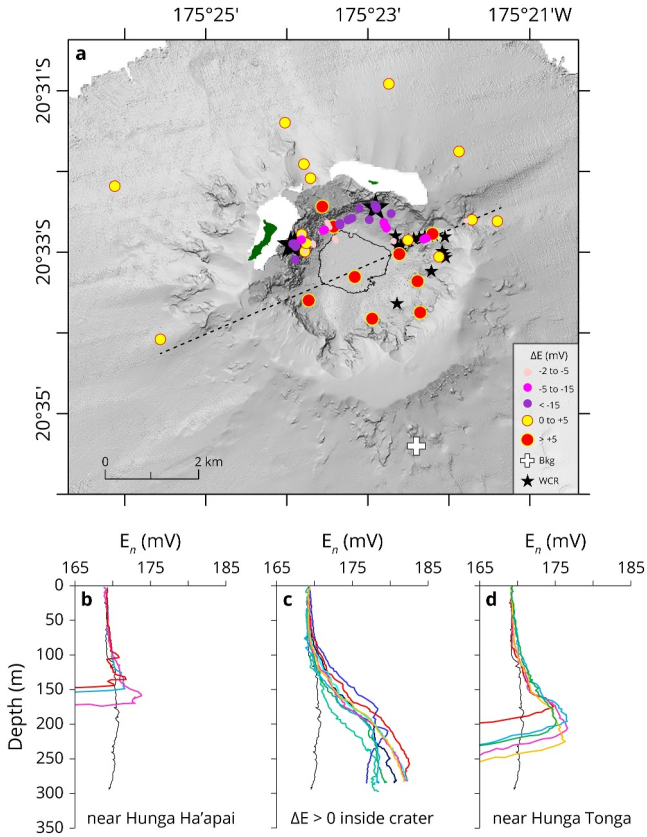

Figure 4. Distribution of oxidation-reduction potential (ORP) anomalies at Hunga volcano during the TESMaP-2 plume survey. (a) Map view shows ΔE inside and outside the crater, regardless of depth. The depth of the greatest magnitude ΔE usually coincided with maximum NTU, but could vary (see text). Negative ΔE values are plotted at locations of anomalies from both vertical casts and tows. Positive ΔE are shown for vertical casts only. The thin black line in each profile plot (b–d) is the vertical cast to the south of Hunga volcano where the regional plume was the weakest, which was used as the "background" station (white "+" symbol in (a) is the same as station 3–6, Figure S2 in Supporting Information S1). The transect aligned with Tow 2 is shown by the dashed black line. Stars are preliminary locations of water column reflectors (i.e., bubble flares; those near the islands have been enlarged for better visibility). Green polygons show the locations of the islands. (b) Profiles of normalized ORP (E_n) for vertical casts near Hunga Ha'apai island with expanded x-axis scale to more clearly show the positive anomalies which were shallower than the particle plume and negative anomalies (see Figure 3a, lower left inset). (c) Normalized ORP profiles for vertical casts where $\Delta E > +5$ mV within the crater (red symbols in (a)). (d) Profiles of normalized ORP for vertical casts near Hunga Tonga island with expanded x-axis scale to more clearly show the positive anomalies (see Figure 3a, lower right inset).

The most intense plume signals near Hunga Tonga were located 500–800 m south of the island (Figure 3a and Figure S2 in Supporting Information S1). Two of the four vertical casts in this area showed a plume maximum layer (based on ORP anomalies) between 175 and 260 m where $\Delta E_{max} = -33$ mV, but for the other two casts the ORP values decreased continuously from ~200 m to the deepest reach of the casts (~295 m). The particle plume at these stations was similar to the distribution seen throughout most of the crater (i.e., increasing deeper than ~150 m, and reaching maximum NTU values of 0.8–1.0 at 200 m and below, with no layered structure; Figure 3a and Figure S4 in Supporting Information S1). These stations were adjacent to the steep, inside crater wall descending from Hunga Tonga island (30°–70°) but located where the seafloor depth ranged from 350 to 650 m. The plume distributions thus suggest a venting source deeper than 270 m in this area. The tow transect between the islands (Tow-3, Figure 3a) shows the depth difference between plumes originating near each island.

The third area with intense turbidity inside the crater was near the ENE wall breach (Figure 3b). The most intense turbidity seen during the expedition (NTU = 1.75) occurred in the deepest 20 m at station 1–6 (cast maximum depth = 283 m). This particle plume did not have a negative ORP anomaly associated with it, but instead had a positive anomaly ($\Delta E = +7.5$ mV). Several WCRs were reported in this area, which along with the positive ORP anomalies suggest active degassing dominated by CO_2.

Significant positive ORP anomalies (up to $\Delta E = +10$ mV) were correlated with turbidity maxima along, and south of, the transect defined by Tow 2 (Figure 4 and Figure S2 in Supporting Information S1). Negative ORP anomalies were only observed along the north inside crater wall near the islands, as described above. These data suggest, that ongoing hydrothermal and/or volcanic activity was occurring near (and possibly between) the islands, but that CO_2 degassing dominated elsewhere within the crater.

Carbon dioxide is one of the most common magmatic gasses and is often emitted at submarine hydrothermal and eruptive vents (e.g., Chadwick, Cashman, et al., 2008; Lupton et al., 2006). Chadwick et al. (2014) observed CO_2 bubbles emerging from the eruptive vents at NW Rota-1 detach from the syneruptively generated sulfur-rich plumes and rise higher in the water column before eventually dissolving. Our observations provide evidence that CO_2 appears to behave similarly at Hunga. Positive ORP anomalies were seen near the top, or above, the particle plumes near the islands (Figures 4b and 4d) suggesting that CO_2 bubbles rise separately to these levels before dissolving, while the particle plume is coupled with other dissolved components that evoke a negative ΔE (Figure 3a).

4.2. Plume Distributions Outside the Crater

The widely dispersed midwater particle plume surrounding the flanks of Hunga volcano seen during the April/May 2022 TESMaP-1 study (~200 m water depth where filtered samples contained ash; Seabrook et al., 2023) was still present 2–3 months later during TESMaP-2. Our survey confirmed that this plume originated within the crater and exited from the crater at both breaches, more prominently from the deeper breach on the ENE rim (Figure 5, Movie S1). Outside the crater near the ENE breach, the plume NTU_{max} (1.75) occurred at 250 m with an abrupt lower limit decreasing to background (NTU ~ 0.09) beneath the sharp gradient. This clearly demonstrates the control that the crater rim has on the distribution of the regional plume outside the crater (Figure 5). The plume immediately outside the crater had a positive ORP anomaly ($\Delta E = +3.3$ mV) coincident with the increased turbidity. The plume, located within the depth range of 125–275 m (NTU_{max} centered at 230 m), was diluted as it advected away from the breaches:

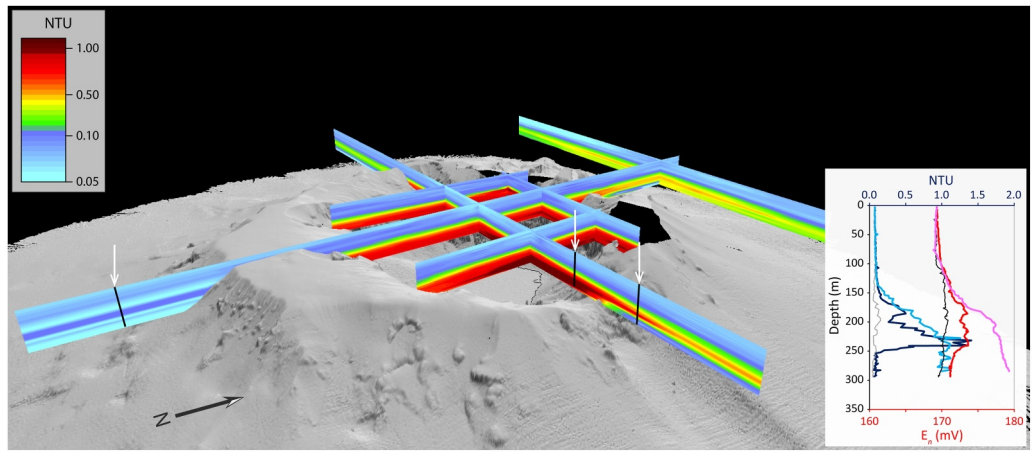

Figure 5. Oblique 3d view (vertical exaggeration = 1.5) of the particle plume inside and outside the crater. Transects shown are tows 1, 2, 3, 4, 6 and 7 (Figure S2 in Supporting Information S1). White arrows at black lines locate the profiles shown in the lower right inset. Profiles in the lower right inset are as follows: dark blue and red = outside crater near breach in E wall (initial downcast of Tow 2); light blue and pink = inside crater near breach in E wall (station 1–5); thin black and gray lines = reference station (3–6) outside and south of the crater. The tow transects and profiles confirm the regional plume originated within the crater, and demonstrate the control the crater rim has on the distribution of the regional plume.

NTU_{max} ~ 0.5 at distances of 1–2 km to the north and east of the volcano, ~0.4 to the west, and only ~0.1 to the south. The positive ORP anomaly magnitudes of the plume decreased similarly.

The presence of the plume dispersing outside the crater during TESMaP-1, three months after the 15 January 2022 eruption, and again during TESMaP-2, is additional evidence that ongoing activity at Hunga volcano persisted for at least 7 months after the 15 January 2022 eruption. Without continual replenishment, we would expect this plume to have decayed or disappeared completely due to dilution, advection by regional currents, and/or the settling of particles within this period of time (e.g., as seen at West Mata; Walker et al., 2019).

5. Discussion

5.1. Volcanic Versus Hydrothermal Activity

It is not possible from these data alone to determine if the sources of the plumes mapped during the TESMaP-2 water column survey were volcanic, hydrothermal, or a combination of both. Eruptive activity does not always accompany hydrothermal activity, but hydrothermal plumes have always been detected at known submarine eruptions, and the spatially limited plume anomalies (NTU ~1; $\Delta E << 0$) near the islands were similar in intensity to plumes over the summits of NW Rota-1 and West Mata when eruptions were directly observed (Walker et al., 2008, 2019). The colocation of WCR, positive ORP anomalies near the upper limits of particle plumes (indicating separate gas phase CO_2 emissions), and intense anomalies of NTU and $\Delta E << 0$ were consistent with what was observed at NW Rota-1 while it was erupting (Chadwick et al., 2014). However, many volcanoes quietly degas for long periods of time between eruptions, and the distribution of positive-only ORP anomalies elsewhere within the crater indicates this was likely happening at Hunga as well.

The extent and physical characteristics of the regional plume outside the crater during TESMaP-2 were comparable to what was seen during TESMaP-1 when ash particles were identified in filtered water samples from the plume (Seabrook et al., 2023). This is additional evidence that there was an eruptive component to the ongoing activity, though probably with a relatively low emission rate. It is not surprising that surface expression of the activity (i.e., discolored water) was not present during either survey because the strongest plume signals were deeper than the thermocline, and the plumes within the crater during TESMaP-2 did not appear to have enough buoyancy to reach the surface.

5.2. Duration of Eruptions

Volcanic activity at Hunga volcano was no longer observable above the ocean surface shortly after the 15 January 2022 climactic event, but many earthquakes (M_w 4.5–5) were detected through 24 January 2022 (Global Volcanism Program, 2022). Similarly, for the March 2009 eruption, acoustic monitoring of the region from January 2009 to April 2010 found that signals consistent with volcanic activity began 7 hr before the first satellite observation and 14 hr before the first eyewitness reports. Visual and acoustic observations led to the assessment that the explosive aspect of the eruption was over within ∼2–3 days; however, acoustic signals indicated that some degree of unrest persisted for at least an additional 3 months through June 2009 (Bohnenstiel et al., 2013).

Discolored water was evident surrounding the merged Hunga Tonga-Hunga Ha'apai island nearly continuously between the end of the 2014/2015 eruption and beginning of the 2021/2022 eruption (Figure S5 in Supporting Information S1), showing that hydrothermal discharge continued between eruptive phases, either through the porous tephra cone, from submerged vents on its shallow flanks (including vents located on the west side of Hunga Ha'apai where the 2009 eruption occurred), or as direct outflow from the crater lake. Changes in the color of the crater lake (ranging from light brown/gray to dark green), and intensity and extent of the discolored water surrounding the island suggest the discharge flux and chemistry was variable (e.g., Urai & Machida, 2005), possibly indicating the influence of magmatic vapor pulses on the hydrothermal system (de Ronde et al., 2005; Stucker et al., 2022). Reactive magmatic gasses (e.g., CO_2, SO_2, HCl, etc.) interact with volcanic rocks and seawater to create mineral deposits that can block porous pathways for gas to escape. Henley et al. (2024), modeled the powerful 15 January 2022 explosive eruption as the result of catastrophic expansion of magmatic gasses that had become trapped and over-pressurized within the edifice. Once the pressure exceeded the strength of the surrounding rock and sealed pathways, the Plinian eruption was inevitable.

Studies of recent eruptions at other nearby volcanoes in Tonga (Home Reef, Late'iti and Volcano"F"; Brandl et al., 2019; Mantas et al., 2011; Vaughan et al., 2007; Yeo et al., 2022), attributed discolored water seen in satellite images to increased hydrothermal venting before and after the times when eruptions were confirmed by steam/ash/tephra plumes or pumice rafts above the surface. The accumulation of deposits sufficient to create ephemeral islands at these sites must obviously have begun while these summits were still submerged, bringing into question the start and end dates based on subaerial plume observations alone. We suggest that the determination of actual eruption start/end dates at shallow submarine volcanoes may be biased by the perceived requirement for observable pumice rafts or plumes injected into the atmosphere. Acknowledging this bias is especially important when considering the activity state of submarine volcanoes for hazard risk assessment. Since not all signs of submarine eruptions reach the surface, it is important to consider what improvements can be made to currently available monitoring and detection capabilities.

5.3. Monitoring Submarine Volcanoes

Methods for monitoring and identifying submarine volcanic eruptions during the past few decades has taken several forms, each with limited effectiveness due to different temporal and spatial scales for detecting events or accessing data. Shallow submarine eruptions have been confirmed in real time by surface expressions visible to humans (including aerial surveys by planes or drones) or satellite observations (e.g., discolored water, pumice rafts, floating lava "balloons," or plumes that breach the surface), which, as noted above, may not accurately define the start and end times of eruptions. Deeper eruptions have been discovered serendipitously when hydrothermal or deep particle plumes with unusual physiochemical characteristics were encountered (Baker et al., 1987, 2011; Resing et al., 2011; Walker et al., 2008), or inferred from analyses of deep ash plume decay (Walker et al., 2019). Seismic networks have detected eruptions (e.g., Baker et al., 2012; Feuillet et al., 2021; Watts et al., 2012; Wright et al., 2008), but existing networks are unable to detect smaller magnitude earthquake swarms at distant volcanoes that can precede eruptions or linger as the energy of the eruptions diminishes (Fox et al., 1993). Military acoustic arrays were at one time accessible for civilian use (Dziak et al., 2012; Fox & Dziak, 1998; Fox et al., 1993), but more recently, hydroacoustic monitoring has relied on deployed hydrophones without real-time access to data (e.g., Dziak et al., 2008, 2012), and the events may be located further than the optimum operational ranges for the arrays' abilities to ascertain source locations with certainty (e.g., Bohnenstiehl et al., 2014). Tsunami warning systems currently focus on earthquake-initiated events, and satellite observations are restricted to detecting surface ocean or atmospheric anomalies, similar to direct human observation, but more effective for remote areas (e.g., Mantas et al., 2011; Urai & Machida, 2005). Repeat bathymetric surveys detect

mass wasting, lava flows, and other deposits, but the time difference between surveys is often on the order of years (e.g., Caress et al., 2012; Chadwick, Wright, et al., 2008; Chadwick et al., 2018, 2019; Embley et al., 2014; Herrera et al., 2023).

One of the first seafloor observatories was installed at Axial volcano (NE Pacific) in 1996. It has provided a wealth of data spanning two eruption cycles (1998–2011–2015) and enabled scientists to predict the approximate timing of future eruptions based on inflation rates and magnitude (Chadwick et al., 2012). Since 2015, data from this observatory have been accessible in real-time, but installations such as this are uncommon and would be expensive and difficult to maintain for monitoring many submarine volcanoes, especially along remote volcanic arcs.

Once discovered, there are still many challenges to conducting thorough investigations of submarine eruptions, but when responses have been possible, valuable information has been obtained about eruptive styles, duration, and rates (Rubin et al., 2012), impacts to ocean chemistry (e.g., Baker et al., 2011; Baumberger et al., 2014; Resing et al., 2011), and ecological impacts (e.g., Barone et al., 2022; Fraile-Nuez et al., 2012; Herrera et al., 2023; Spietz et al., 2018). The directly observed eruptions at NW Rota-1 (500–550 m, Mariana arc) and West Mata (1,200 m, NE Lau) were nearly continuous over the span of multiple years, though with relatively low eruption rates and no visible impact at the ocean surface (Chadwick, Cashman, et al., 2008; Embley et al., 2014; Schnur et al., 2017), but Havre volcano (720–1,220 m, Kermadec arc) produced an extensive pumice raft and brief atmospheric plume during an eruption thought to last just a few days (R. J. Carey et al., 2014).

Physical and chemical impacts to the ocean due to submarine eruptions, such as multi-year post-eruption invigoration of hydrothermal venting, are effectively investigated by utilizing hydrothermal plume surveys (e.g., Baker et al., 1987, 2012, 2019, and references therein). Magmatic gas flux measurements are key parameters at most subaerial volcano observatories where measurable changes have been observed before, during and after eruptions (e.g., Aiuppa et al., 2023; McGee et al., 2008). Repeat hydrothermal plume surveys at submarine volcanoes can provide similar, crucial data for understanding the activity status of submarine volcanoes and identifying changes that may be occurring. For example, plume surveys at Brothers submarine volcano (Kermadec arc) have shown the influence that pulses of magmatic vapor have on the intensity and chemistry of hydrothermal discharge (de Ronde et al., 2005; Stucker et al., 2022; Walker and de Ronde, 2023).

Water column surveys and sampling can also be useful tools for monitoring the recovery and evolution of ecosystems after volcanic eruptions. At Hunga volcano, ongoing activity, whether volcanic or hydrothermal, and accumulation or removal of the crater contents will influence the physical and chemical conditions within the crater and affect the reestablishment of flora and fauna in this entirely new habitat created by the eruption. If water within the crater continues to remain isolated and accumulate CO_2, acidity and density will increase (e.g., S. Carey et al., 2013, references therein) further inhibiting vertical circulation and exchange with the surrounding ocean. Ecosystem recovery could be limited to microbial species that can tolerate more acidic conditions, as seen at Kolumbo volcano where pH has been measured as low as ∼5 (Santorini volcanic field, Greece; S. Carey et al., 2013; Kilias et al., 2013), or lead to death of intolerant species that inadvertently become trapped, such as at Vailulu'u (American Samoa; Staudigel et al., 2006). Comparing the ecological recovery within the newly excavated crater, where more hostile or extreme conditions may persist, to the new habitat created by thick ash deposits outside the crater and exposed to open ocean conditions (Seabrook et al., 2023), will provide valuable new information about the impact of this eruption, specifically, and the resilience of deep-sea ecosystems to dramatic disturbances more generally (e.g., Herrera et al., 2023). This site, and others like it (e.g., Kolumbo volcano, Greece), may also be considered ideal natural laboratories for studying ecosystem responses and resilience to increased ocean acidification due to climate change (Mandalakis et al., 2019).

The increased availability and advances in autonomous and remotely controlled vehicles, such as USV *Maxlimer*, will expand our capabilities to monitor submarine volcanoes efficiently, effectively and safely, to improve our understanding of volcanic processes along with their potential hazards, and possibly provide capabilities for early detection of hazardous eruptions.

6. Summary

This study showed there was ongoing activity at Hunga volcano 7 months after the powerfully explosive 15 January 2022 eruption. Hydrothermal and/or volcanic venting was identified by intense particle and chemical

anomalies located along the steep inside walls of the crater near the remnants of both islands. CO_2 degassing appeared to dominate elsewhere within the crater. Water within the crater is isolated from water masses outside the crater, with exchange limited to the breaches in the crater rim located between the islands on the northern side, and SE of Hunga Tonga on the ENE side. The shallow rim (<100 m) surrounding the other 75% of the crater circumference ensures that both dissolved and particulate products of ongoing activity are trapped within the crater. With time, increases in turbidity and acidity may create an extreme, and possibly hostile, environment to many species, which will impact ecological recovery.

Outside the crater, the plume was detected in all directions within the 150–300 m depth range. It was most intense adjacent to the ENE breach and to the north of the volcano. This is consistent with the plume originating within the crater, escaping through the breaches, and then being advected by regional currents around the summit. When this plume was first observed during the TESMaP-1 expedition (3–4 months post-eruption), fine fresh ash fragments were found in filtered seawater samples (Seabrook et al., 2023). The similarity of the intensity and distribution of this regional plume between April 2022 and August 2022 suggests that the level and style of activity did not diminish significantly during that time interval.

Infrequent but extremely powerful explosive eruptions of submarine volcanoes can pose significant hazards both near and far from the volcano. Many of the volcanoes along the Tonga sector of the arc are near populated areas that can, and have, experienced significant impacts from eruptions. Since the 15 January 2022 eruption of Hunga volcano, Home Reef, located 180 km NE of Hunga, has erupted at least twice (September 2022 and October 2023; Global Volcanism Program, 2023). The start of the September 2022 eruption was noted as 10 September when satellite images showed a steam plume and emergence of new volcanic deposits above sea level. However, satellite images also showed discolored water at this location beginning in late May 2022, which likely indicated the actual start of the eruption since new material needed to be deposited below sea level before Home Reef could emerge as a new island. Assessments of start and end times of shallow submarine eruptions is likely biased by the assumption that an eruption is not in progress if there are no dramatic indicators at or above the ocean surface.

Additional investment in infrastructure, analytical capabilities, and research is needed to improve monitoring systems for accurate reporting, and potential prediction of hazardous submarine eruptions. For example, the installation of optimally placed hydroacoustic and seismic arrays that deliver real-time data to local hazard managers and the development of warning systems that recognize volcanogenic tsunamis would be beneficial.

Autonomous platforms are increasingly affordable, energy efficient, and available, and are already playing a major role in monitoring changing ocean conditions globally. The novel application of remotely controlled uncrewed vessel technology, used for the first time in this study, to conduct truly over-the-horizon bathymetric and water column surveys >16,000 km away from the study site was remarkably successful. Major advantages included (a) reduced risk to personnel and equipment, (b) an estimated 98% reduction in the amount of fuel that a typical survey vessel would use, and (c) fewer personnel were required to travel from around the world to crew the vessel (i.e., additional fuel savings). This study is an important demonstration of the potential of this innovative technology to contribute to broader applications in ocean exploration, monitoring, and event response.

7. Inclusion in Global Research Statement

Fieldwork was conducted mere months after communities in the Kingdom of Tonga were severely impacted by one of the most powerful explosive volcanic eruptions of the last 300 years. The Kingdom of Tonga granted permission to conduct operations within their territorial waters and were supportive of the effort to understand the submarine impacts of this major volcanic eruption. The Ministry of Lands and Natural Resources approved the Research Permit and provided logistic support during operations. We appreciate the participation of all individuals involved given the difficult post-eruption conditions complicated further by COVID-19 pandemic-related concerns and restrictions.

Data Availability Statement

The MAPR data used in this study (Walker and de Ronde, 2024) is available for FAIR sharing and download at https://www.marine-geo.org/doi/10.60521/331769. The data in Table 1 is available via the Eruption data base of the Global Volcanism Program at https://volcano.si.edu/search_eruption.cfm.

Acknowledgments
We would like to first and foremost thank the Kingdom of Tonga for their permission to conduct operations within their territorial waters and support of this project. We thank the entire SEA-KIT team for their positive, can-do approach to the mission and persistence to overcome any unexpected operational challenges, and the multibeam mapping survey team for providing critical seafloor depth information during real-time operations. We thank Phin Franklin and Chris Lacey for skillfully managing MAPR requirements in the field. We thank Robin Falconer for connecting us with the opportunity to add water column sampling to the project, and Mike Williams and Kevin Mackay for providing valuable support from NIWA. We thank Sean McAllister, Paraskevi Nomikou, an anonymous reviewer, and editor Marie Edmonds for their time and thoughtful comments to improve the manuscript. The TESMaP project was funded by the Nippon Foundation and managed by NIWA. CEJdR was funded by GNS Science through the New Zealand Strategic Science Investment Fund (SSIF). SLW was funded by the Earth-Ocean Interactions program at NOAA-PMEL. This is PMEL contribution number 5613.

References

Aiuppa, A., Lo Bue Trisciuzzi, G., Alparone, S., Bitetto, M., Coltelli, M., Delle Donne, D., et al. (2023). A SO_2 flux study of the Etna volcano 2020–2021 paroxysmal sequences. *Frontiers in Earth Science*, *11*, 1115111. https://doi.org/10.3389/feart.2023.1115111

Arculus, R. J. (2006). Northern Tonga arc and Fonualei Rifts: Initial results from the NoToVE (SS11/2004) research voyage. In *ASEG Extended Abstracts, 2006:1* (pp. 1–5). https://doi.org/10.1071/ASEG2006ab150

Baker, E. T., Chadwick, W. W., Cowen, J. P., Dziak, R. P., Rubin, K. H., & Fornari, D. J. (2012). Hydrothermal discharge during submarine eruptions: The importance of detection, response and new technology. *Oceanography*, *25*(1), 128–141. https://doi.org/10.5670/oceanog.2012.11

Baker, E. T., Feely, R. A., de Ronde, C. E. J., Massoth, G. J., & Wright, I. C. (2003). Submarine hydrothermal venting on the southern Kermadec volcanic arc front (offshore New Zealand): Location and extent of particle plume signatures. In R. D. Larter & P. T. Leat (Eds.), *Intra-oceanic subduction systems: Tectonic and magmatic processes* (pp. 141–161). Special Publications, 219, Geological Society.

Baker, E. T., Lupton, J. E., Resing, J. A., Baumberger, T., Lilley, M. D., Walker, S. L., & Rubin, K. H. (2011). Unique event plumes from a 2008 eruption on the Northeast Lau spreading center. *Geochemistry, Geophysics, Geosystems*, *12*(9), Q0AF02. https://doi.org/10.1029/2011GC003725

Baker, E. T., Massoth, G. J., & Feely, R. A. (1987). Cataclysmic hydrothermal venting on the Juan de Fuca Ridge. *Nature*, *329*(6135), 149–151. https://doi.org/10.1038/329149a0

Baker, E. T., Resing, J. A., Haymon, R. M., Tunnicliffe, V., Lavelle, J. W., Martinez, F., et al. (2016). How many vent fields? New estimates of vent field populations on ocean ridges from precise mapping of hydrothermal discharge locations. *Earth and Planetary Science Letters*, *449*, 186–196. https://doi.org/10.1016/j.epsl.2016.05.031

Baker, E. T., Tennant, D. A., Feely, R. A., Lebon, G. T., & Walker, S. L. (2001). Field and laboratory studies on the effect of particle size and composition on optical backscattering measurements in hydrothermal plumes. *Deep Sea Research Part I*, *48*(2), 593–604. https://doi.org/10.1016/S0967-0637(00)00011-X

Baker, E. T., Walker, S. L., Chadwick, W. W., Butterfield, D. A., Buck, N. J., & Resing, J. A. (2019). Post eruption enhancement of hydrothermal activity: A 33-year, multieruption time series at Axial Seamount (Juan de Fuca Ridge). *Geochemistry, Geophysics, Geosystems*, *20*(2), 814–828. https://doi.org/10.1029/2018GC007802

Barone, B., Letelier, R. M., Rubin, K. H., & Karl, D. M. (2022). Satellite detection of a massive phytoplankton bloom following the 2022 submarine eruption of the Hunga Tonga-Hunga Ha'apai volcano. *Geophysical Research Letters*, *49*(17), e2022GL099293. https://doi.org/10.1029/2022GL099293

Baumberger, T., Lilley, M. D., Lupton, J. E., Baker, E. T., Resing, J. A., Buck, N. J., et al. (2020). Dissolved gas and metal composition of hydrothermal plumes from a 2008 submarine eruption on the Northeast Lau Spreading Center. *Frontiers in Marine Science*, *7*, 171. https://doi.org/10.3389/fmars.2020.00171

Baumberger, T., Lilley, M. D., Resing, J. A., Lupton, J. E., Baker, E. T., Butterfield, D. A., et al. (2014). Understanding a submarine eruption through time series hydrothermal plume sampling of dissolved and particulate constituents: West Mata, 2008–2012. *Geochemistry, Geophysics, Geosystems*, *15*(12), 4631–4650. https://doi.org/10.1002/2014GC005460

Bohnenstiehl, D. R., Dziak, R. P., Matsumoto, H., & Conder, J. (2014). Acoustic response of submarine volcanoes in the Tofua Arc and northern Lau Basin to two great earthquakes. *Geophysical Journal International*, *196*(3), 1657–1675. https://doi.org/10.1093/gji/ggt472

Bohnenstiehl, D. R., Dziak, R. P., Matsumoto, H., & Lau, T.-K. (2013). Underwater acoustic records from the March 2009 eruption of Hunga Ha'apai–Hunga Tonga volcano in the Kingdom of Tonga. *Journal of Volcanology and Geothermal Research*, *249*, 12–24. https://doi.org/10.1016/j.jvolgeores.2012.08.014

Brandl, P. A., Schmid, F., Augustin, N., Grevemeyer, I., Arculus, R. J., Devey, C. W., et al. (2019). The 6–8 Aug 2019 eruption of 'volcano F' in the Tofua arc, Tonga. *Journal of Volcanology and Geothermal Research*, *390*, 106695. https://doi.org/10.1016/j.jvolgeores.2019.106695

Brenna, M., Cronin, S. J., Smith, I. E., Pontesilli, A., Tost, M., Barker, S., et al. (2022). Post-caldera volcanism reveals shallow priming of an intra-ocean arc andesitic caldera: Hunga volcano, Tonga, SW Pacific. *Lithos*, *412*, 106614. https://doi.org/10.1016/j.lithos.2022.106614

Caress, D. W., Clague, D. A., Paduan, J. B., Martin, J., Dreyer, B., Chadwick, W. W., Jr., et al. (2012). Repeat bathymetric surveys at 1-metre resolution of lava flows erupted at Axial Seamount in April 2011. *Nature Geoscience*, *5*(7), 483–488. https://doi.org/10.1038/ngeo1496

Carey, R. J., Wysoczanski, R., Wunderman, R., & Jutzeler, M. (2014). Discovery of the largest historic silicic submarine eruption. *EOS Transactions*, *95*(19), 157–164. https://doi.org/10.1002/2014EO190001

Carey, S., Nomikou, P., Croff Bell, K., Lilley, M., Lupton, J., Roman, C., et al. (2013). CO_2 degassing from hydrothermal vents at Kolumbo submarine volcano, Greece, and the accumulation of acidic crater water. *Geology*, *41*(9), 1035–1038. https://doi.org/10.1130/G34286.1

Carvajal, M., Sepúlveda, I., Gubler, A., & Garreaud, R. (2022). Worldwide signature of the 2022 Tonga volcanic tsunami. *Geophysical Research Letters*, *49*(6), e2022GL098153. https://doi.org/10.1029/2022GL098153

Chadwick, W. W., Jr., Cashman, K. V., Embley, R. W., Matsumoto, H., Dziak, R. P., de Ronde, C. E. J., et al. (2008). Direct video and hydrophone observations of submarine explosive eruptions at NW Rota-1 Volcano, Mariana Arc. *Journal of Geophysical Research*, *113*(B8), B08S10. https://doi.org/10.1029/2007JB005215

Chadwick, W. W., Jr., Merle, S. G., Baker, E. T., Walker, S. L., Resing, J. A., Butterfield, D. A., et al. (2018). A recent volcanic eruption discovered on the central Mariana back-arc spreading center. *Frontiers in Earth Science*, *6*, 172. https://doi.org/10.3389/feart.2018.00172

Chadwick, W. W., Jr., Merle, S. G., Buck, N. J., Lavelle, J. W., Resing, J. A., & Ferrini, V. (2014). Imaging of CO_2 bubble plumes above an erupting submarine volcano, NW Rota-1, Mariana Arc. *Geochemistry, Geophysics, Geosystems*, *15*(11), 4325–4342. https://doi.org/10.1002/2014GC005543

Chadwick, W. W., Jr., Nooner, S. L., Butterfield, D. A., & Lilley, M. D. (2012). Seafloor deformation and forecasts of the April 2011 eruption at axial seamount. *Nature Geoscience*, *5*(7), 474–477. https://doi.org/10.1038/ngeo1464

Chadwick, W. W., Jr., Rubin, K. H., Merle, S. G., Bobbitt, A. M., Kwasnitschka, T., & Embley, R. W. (2019). Recent eruptions between 2012 and 2018 discovered at West Mata submarine volcano (NE Lau Basin, SW Pacific) and characterized by new ship, AUV, and ROV data. *Frontiers in Marine Science*, *6*, 495. https://doi.org/10.3389/fmars.2019.00495

Chadwick, W. W., Jr., Wright, I. C., Schwarz-Schampera, U., Hyvernaud, O., Reymond, D., & de Ronde, C. E. J. (2008). Cyclic eruptions and sector collapses at Monowai submarine volcano, Kermadec arc: 1998–2007. *Geochemistry, Geophysics, Geosystems*, *9*(10), Q10014. https://doi.org/10.1029/2008GC002113

Clare, M. A., Yeo, I. A., Watson, S., Wysoczanski, R., Seabrook, S., Mackay, K., et al. (2023). Fast and destructive density currents created by ocean-entering volcanic eruptions. *Science*, *381*(6662), 1085–1092. https://doi.org/10.1126/science.adi3038

Cronin, S., & Tonga Geoological Services. (2022). Hunga Tonga-Hunga Ha'apai volcano (Tonga): New bathymetry map of caldera. Retrieved from https://www.volcanodiscovery.com/hunga-tonga-hunga-haapai/news/181524/Hunga-Tonga-Hunga-Ha-apai-volcano-Tonga-new-bathymetry-map-of-caldera.html

de Ronde, C. E. J. (2022). When science doesn't go to plan: Research voyage to Hunga Tonga-Hunga Ha'apai volcano cut short. Retrieved from https://youtu.be/vc-Y8xjhdFw

de Ronde, C. E. J., Baker, E. T., Massoth, G. J., Lupton, J. E., Wright, I. C., Feely, R. A., & Greene, R. R. (2001). Intra-oceanic subduction-related hydrothermal venting, Kermadec volcanic arc, New Zealand. *Earth and Planetary Science Letters*, *193*(3–4), 359–369. https://doi.org/10.1016/S0012-821X(01)00534-9

de Ronde, C. E. J., Hannington, M. D., Stoffers, P., Wright, I. C., Ditchburn, R. G., Reyes, A. G., et al. (2005). Evolution of a submarine magmatic-hydrothermal system: Brothers volcano, southern Kermadec arc, New Zealand. *Economic Geology*, *100*(6), 1097–1133. https://doi.org/10.2113/100.6.1097

Dziak, R. P., Baker, E. T., Shaw, A. M., Bohnenstiehl, D. R., Chadwick, W. W., Jr., Haxel, J. H., et al. (2012). Flux measurements of explosive degassing using a year-long hydroacoustic record at an erupting submarine volcano. *Geochemistry, Geophysics, Geosystems*, *13*(11), Q0AF07. https://doi.org/10.1029/2012GC004211

Dziak, R. P., Haxel, J. H., Matsumoto, H., Lau, T. K., Merle, S. M., de Ronde, C. E. J., et al. (2008). Observations of local seismicity and harmonic tremor at Brothers Volcano, south Kermadec Arc, using an ocean-bottom hydrophone array. *Journal of Geophysical Research*, *113*(B8), B08S04. https://doi.org/10.1029/2007JB005533

Embley, R. W., Merle, S. G., Baker, E. T., Rubin, K. H., Lupton, J. E., Resing, J. A., et al. (2014). Eruptive modes and hiatus of volcanism at West Mata seamount: NE Lau basin: 1996–2012. *Geochemistry, Geophysics, Geosystems*, *15*(10), 4093–4115. https://doi.org/10.1002/2014GC005387

Ferrini, V. (2022). Bathymetry grid of Hunga Tonga-Hunga Ha'apai Volcano generated from data acquired during Falkor cruise FK160407 (2016). *IEDA*. https://doi.org/10.26022/IEDA/330859

Feuillet, N., Jorry, S., Crawford, W. C., Deplus, C., Thinon, I., Jacques, E., et al. (2021). Birth of a large volcanic edifice offshore Mayotte via lithosphere-scale dyke intrusion. *Nature Geoscience*, *14*(10), 787–795. https://doi.org/10.1038/s41561-021-00809-x

Fox, C. G., & Dziak, R. P. (1998). Hydroacoustic detection of volcanic activity on the Gorda ridge, February–March 1996. *Deep Sea Research Part II*, *45*(12), 2513–2530. https://doi.org/10.1016/S0967-0645(98)00081-2

Fox, C. G., Dziak, R. P., Matsumoto, H., & Schreiner, A. E. (1993). Potential for monitoring low-level seismicity on the Juan de Fuca Ridge using military hydrophone arrays. *Marine Technology Society Journal*, *27*(4), 22–30.

Fraile-Nuez, E., González-Dávila, M., Santana-Casiano, J. M., J. Arístegui, J., Alonso-González, I. J., Hernández-León, S., et al. (2012). The submarine volcano eruption at the Island of El Hierro: Physical-chemical perturbation and biological response. *Scientific Reports*, *2*(1), 486. https://doi.org/10.1038/srep00486

Garvin, J. B., Slayback, D. A., Ferrini, V., Frawley, J., Giguere, C., Asrar, G. R., & Andersen, K. (2018). Monitoring and modeling the rapid evolution of Earth's newest volcanic island: *Hunga Tonga Hunga Ha'apai* (Tonga) using high spatial resolution satellite observations. *Geophysical Research Letters*, *45*(8), 3445–3452. https://doi.org/10.1002/2017GL076621

Global Volcanism Program. (2022). Report on Hunga Tonga-Hunga Ha'apai (Tonga). In K. L. Bennis, & E. Venzke (Eds.) *Bulletin of the global volcanism network* (Vol. 47, p. 3), Smithsonian Institution. Retrieved from https://volcano.si.edu/showreport.cfm?doi=10.5479/si.GVP.BGVN202203-243040

Global Volcanism Program. (2023). *Home Reef (243080) in (Database) volcanoes of the world (v. 5.1.5; 15 December 2023)*. Smithsonian Institution, Compiled by Venzke, E. https://doi.org/10.5479/si.GVP.VOTW5-2023.5.1

Global Volcanism Program. (2024). *(Database) volcanoes of the world (v. 5.1.7; 26 April 2024)*. Smithsonian Institution, Compiled by Venzke, E.

Henley, R. W., de Ronde, C. E. J., Arculus, R. J., Hughes, G., Pham, T.-S., Casas, A. S., et al. (2024). The 15 January 2022 Hunga (Tonga) eruption: A gas-driven climactic explosion. *Journal of Volcanology and Geothermal Research*, *451*, 108077. https://doi.org/10.1016/j.jvolgeores.2024.108077

Herrera, S., Chadwick, W. W., Jr., Jackson, M. G., Konter, J., McCartin, L., Pittoors, N., et al. (2023). From basalt to biosphere: Early non-vent community succession on the erupting Vailulu'u deep seamount. *Frontiers in Marine Science*, *10*, 1110062. https://doi.org/10.3389/fmars.2023.1110062

Kadko, D. C., Rosenberg, N. D., Lupton, J. E., Collier, R. W., & Lilley, M. D. (1990). Chemical reaction rates and entrainment within the Endeavour Ridge hydrothermal plume. *Earth and Planetary Science Letters*, *99*(4), 315–335. https://doi.org/10.1016/0012-821X(90)90137-M

Kilias, S. P., Nomikou, P., Papanikolaou, D., Polymenakou, P. N., Godelitsas, A., Argyraki, A., et al. (2013). New insights into hydrothermal vent processes in the unique shallow-submarine arc-volcano, Kolumbo (Santorini), Greece. *Scientific Reports*, *3*(1), 2321. https://doi.org/10.1038/srep02421

Kubota, T., Tatsuhiko, S., & Nishida, K. (2022). Global fast-traveling tsunamis driven by atmospheric Lamb waves on the 2022 Tonga eruption. *Science*, *377*(6601), 91–94. https://doi.org/10.1126/science.abo4364

Le Mevel, H., Miller, C. A., Ribó, M., Cronin, S., & Kula, T. (2023). The magmatic system under Hunga volcano before and after the 15 January 2022 eruption. *Science Advances*, *9*(50), eadh3156. https://doi.org/10.1126/sciadv.adh3156

Lipman, P. W. (2000). *Calderas. Encyclopedia of volcanoes* (pp. 643–662). Academic Press.

Lupton, J., Butterfield, D., Lilley, M., Evans, L., Nakamura, K.-I., Chadwick, W., Jr., et al. (2006). Submarine venting of liquid carbon dioxide on a Mariana Arc volcano. *Geochemistry, Geophysics, Geosystems*, *7*(8), Q08007. https://doi.org/10.1029/2005GC001152

Lynette, P., McCann, M., Zhou, Z., Renteria, W., Borrero, D. G., Fa'anunu, O., et al. (2022). Diverse Tsunami genesis triggered by the Hunga Tonga-Hunga Ha'apai eruption. *Nature*, *609*(7928), 728–733. https://doi.org/10.1038/s41586-022-05170-6

Mackay, K. (2022). Digital elevation models of Hunga volcano; pre- and post- 15 January 2022 eruption (1.0) [Dataset]. *Zenodo*. https://doi.org/10.5281/zenodo.7456324

Mackay, K., Clark, M. R., Seabrook, S., Armstrong, E., Barr, N., Frontin-Rollet, G., et al. (2022). Environmental impacts of the 2022 eruption of Hunga Tonga–Hunga Ha'apai: Voyage report of part 1 of the TESMaP survey of the region in April–May 2022 (TAN2206). In *NIWA Technical Report No. 141* (p. 197). https://doi.org/10.13140/RG.2.2.24952.62727

Mandalakis, M., Gavriilidou, A., Polymenakou, P. N., Christakis, C. A., Nomikou, P., Medvecky, M., et al. (2019). Microbial strains isolated from CO_2-venting Kolumbo submarine volcano show enhanced co-tolerance to acidity and antibiotics. *Marine Environmental Research*, *144*, 102–110. https://doi.org/10.1016/j.marenvres.2019.01.002

Mantas, V. M., Pereira, A. J. S. C., & Morais, P. V. (2011). Plumes of discolored water of volcanic origin and possible implications for algal communities. The case of the Home Reef eruption of 2006 (Tonga, Southwest Pacific Ocean). *Remote Sensing of Environment*, *115*(6), 1341–1352. https://doi.org/10.1016/j.rse.2011.01.014

Massoth, G. J., Baker, E. T., Worthington, T., Lupton, J. E., de Ronde, C., Arculus, R. A., et al. (2007). Multiple hydrothermal sources along the south Tonga arc and Valu Fa Ridge. *Geochemistry, Geophysics, Geosystems*, *8*(11), Q11008. https://doi.org/10.1029/2007GC001675

Matoza, R. S., Fee, D., Assink, J. D., Iezzi, A. M., Green, D. N., Kim, K., et al. (2022). Atmospheric waves and global seismoacoustic observations of the January 2022 Hunga eruption, Tonga. *Science*, *377*(6601), 95–100. https://doi.org/10.1126/science.abo7063

Mazot, A., Schwandner, F. M., Christian, B., de Ronde, C. E. J., Inguaggiato, S., Scott, B., et al. (2014). CO_2 discharge from the bottom of volcanic Lake Rotomahana, New Zealand. *Geochemistry, Geophysics, Geosystems*, *15*(3), 577–588. https://doi.org/10.1002/2013GC004945

McGee, K. A., Doukas, M. P., McGimsey, R. G., Neal, C. A., & Wessels, R. L. (2008). Atmospheric contribution of gas emissions from Augustine volcano, Alaska during the 2006 eruption. *Geophysical Research Letters*, *35*(3), L03306. https://doi.org/10.1029/2027GL032301

Merle, S. G., Embley, R. W., Johnson, H. P., Lau, T.-K., Phrampus, B. J., Raineault, N. A., & Gee, L. J. (2021). Distribution of methane plumes on Cascadia Margin and implications for the landward limit of methane hydrate stability. *Frontiers in Earth Science*, *9*, 531714. https://doi.org/10.3389/feart.2021.531714

Nakano, U., Hanzawa, M., Marumo, R., & Fukuoka, J. (1954). Oceanographic features of a submarine eruption that destroyed the Kaiyo-maru N0. 5. *Journal of Marine Research*, *13*(1), 48–66.

NASA. (2022). *Tonga volcano plume reached the mesosphere*. National Aeronautics and Space Administration. Retrieved from https://earthobservatory.nasa.gov/images/149474/tonga-volcano-plume-reached-the-mesosphere

NIWA-Nippon Foundation Tonga Eruption Seabed Mapping Project (TESMaP). (2023). Digital elevation models of Hunga volcano, Tonga, from the MAX2201 voyage, July–August 2022 [Dataset]. *Zenodo*. https://doi.org/10.5281/zenodo.10038898

NOAA. (2022). Hunga Tonga-Hunga Ha'apa volcano-generated Tsunami, January 15, 2022. National Oceanic and Atmospheric Administration, Pacific Marine Environmental Laboratory, NOAA Center for Tsunami Research. Retrieved from https://nctr.pmel.noaa.gov/tonga20220115

Poli, P., & Shapiro, N. M. (2022). Rapid characterization of large volcanic eruptions: Measuring the impulse of the Hunga Tonga Ha'apai explosion from teleseismic waves. *Geophysical Research Letters*, *49*(8), e2022GL098123. https://doi.org/10.1029/2022GL098123

Proud, S. R., Prata, A. T., & Schmauß, S. (2022). The January 2022 eruption of Hunga Tonga-Hunga Ha'apai volcano reached the mesosphere. *Science*, *378*(6619), 554–557. https://doi.org/10.1126/science.abo4076

Resing, J. A., Baker, E. T., Lupton, J. E., Walker, S. L., Butterfield, D. A., Massoth, G. J., & Nakamura, K.-I. (2009). Chemistry of hydrothermal plumes above submarine volcanoes of the Mariana Arc. *Geochemistry, Geophysics, Geosystems*, *10*(2), Q02009. https://doi.org/10.1029/2008GC002141

Resing, J. A., Rubin, K. H., Embley, R. W., Lupton, J. E., Baker, E. T., Dziak, R. P., et al. (2011). Active submarine eruption of Boninite in the northeastern Lau Basin. *Nature Geoscience*, *4*(11), 799–806. https://doi.org/10.1038/NGEO1275

Ribo, M., Cronin, S., Stern, S., Park, S.-H., Garvin, J., & Kula, T. (2023). Morphological evolution of the Hunga Tonga–Hunga Ha'apai submarine volcano after the explosive eruption. In *EGU general assembly 2023, Vienna, Austria, 24–28 April 2023, EGU23-17221*. https://doi.org/10.5194/egusphere-egu23-17221

Rubin, K. H., Soule, S. A., Chadwick, W. W., Fornari, D. J., Clague, D. A., Embley, R. W., et al. (2012). Volcanic eruptions in the deep sea. *Oceanography*, *25*(1), 142–157. https://doi.org/10.5670/oceanog.2012.12

Schnur, S. R., Chadwick, W. W., Embley, R. W., Ferrini, V. L., de Ronde, C. E. J., Cashman, K. V., et al. (2017). A decade of volcanic construction and destruction at the summit of NW Rota-1 seamount: 2004–2014. *Journal of Geophysical Research: Solid Earth*, *122*(3), 1558–1584. https://doi.org/10.1002/2016JB013742

Seabrook, S., Mackay, K., Watson, S. J., Clare, M. A., Hunt, J. E., Yeo, I. A., et al. (2023). Volcaniclastic density currents explain widespread and diverse seafloor impacts of the 2022 Hunga Volcano eruption. *Nature Communications*, *14*(1), 7881. https://doi.org/10.1038/s41467-023-43607-2

Smith, I. E. M., & Price, R. C. (2006). The Tonga-Kermadec arc and Havre-Lau back-arc system: Their role in the development of tectonic and magmatic models for the western Pacific. *Journal of Volcanology and Geothermal Research*, *156*(3–4), 315–331. https://doi.org/10.1016/j.jvolgeores.2006.03.006

Spietz, R. L., Butterfield, D. A., Buck, N. J., Larson, B. I., Chadwick, W. W., Jr., Walker, S. L., et al. (2018). Deep-sea volcanic eruptions create unique chemical and biological linkages between the subsurface lithosphere and oceanic hydrosphere. *Oceanography*, *31*(1), 128–135. https://doi.org/10.5670/oceanog.2018.120

Statham, P. J., German, C. R., & Connelly, D. P. (2005). Iron (II) distribution and oxidation kinetics in hydrothermal plumes at the Kairei and Edmond vent sites, Indian Ocean. *Earth and Planetary Science Letters*, *236*(3–4), 588–596. https://doi.org/10.1016/j.epsl.2005.03.008

Staudigel, H., Hart, S. R., Koppers, A. A. P., Constable, C., Workman, R., Kurz, M., & Baker, E. T. (2004). Hydrothermal venting at Vailulu'u Seamount: The smoking end of the Samoan chain. *Geochemistry, Geophysics, Geosystems*, *5*(2), Q02003. https://doi.org/10.1029/2003GC000626

Staudigel, H., Hart, S. R., Pile, A., Bailey, B. E., Baker, E. T., Brooke, S., et al. (2006). Vailulu'u Seamount, Samoa: Life and death on an active submarine volcano. *Proceedings of the National Academy of Sciences*, *103*(17), 6448–6453. https://doi.org/10.1073/pnas.0600830103

Stern, R. (2022). There's a hole in the Bottom of the sealmapping the Hunga Tonga—Hunga Ha'apai Caldera, YouTube, uploaded by UTD Geosciences Studio, 16 October 2022. Retrieved from https://youtu.be/i38DkgU0f7s

Stucker, V. K., de Ronde, C. E. J., Laurence, K. J., & Phillips, A. M. (2022). Rare time series of hydrothermal fluids for a submarine volcano: 14 years of vent fluid compositions for Brothers volcano, Kermadec arc, New Zealand. *Economic Geology*, *118*(7), 1563–1576. https://doi.org/10.5382/econgeo.4922

Urai, M., & Machida, S. (2005). Discolored seawater detection using ASTER reflectance products: A case study of Satsuma-Iwojima, Japan. *Remote Sensing of Environment*, *99*(1–2), 95–104. https://doi.org/10.1016/j.rse.2005.04.028

Vaughan, R. G., Abrams, M. J., Hook, S. J., & Pieri, D. C. (2007). Satellite observations of new volcanic island in Tonga. *EOS*, *88*(4), 37–41. https://doi.org/10.1029/2007EO040002

Walker, S. L. (2023). MAPR: PMEL's Miniature autonomous plume Recorder. *Oceanography*, *36*(2–3), 212–215. https://doi.org/10.5670/oceanog.2023.220

Walker, S. L., Baker, E. T., Lupton, J. E., & Resing, J. A. (2019). Patterns of fine ash dispersal related to volcanic activity at West Mata volcano, NE Lau basin. *Frontiers in Marine Science*, *6*, 593. https://doi.org/10.3389/fmars.2019.00593

Walker, S. L., Baker, E. T., Resing, J. A., Chadwick, W. W., Jr., Lebon, G. T., Lupton, J. E., & Merle, S. G. (2008). Eruption-fed particle plumes and volcaniclastic deposits at a submarine volcano: NW Rota-1, Mariana arc. *Journal of Geophysical Research*, *113*(B8), B08S11. https://doi.org/10.1029/2007JB005441

Walker, S. L., Baker, E. T., Resing, J. A., Nakamura, K., & McLain, P. D. (2007). A new tool for detecting hydrothermal plumes: An ORP sensor for the PMEL MAPR. In *EOS, Transactions of the American Geophysical Union, volume 88(52), fall meeting supplement, abstract V21D-0753*.

Walker, S. L., & de Ronde, C. (2024). Miniature autonomous plume Recorder (MAPR) data acquired at Hunga volcano, Kingdom of Tonga in July-August 2022 during phase 2 of the Tonga eruption seabed mapping project (TESMaP-2) [Dataset]. *MGDS*. https://doi.org/10.60521/331769

Walker, S. L., & de Ronde, C. E. J. (2023). Two decades of monitoring hydrothermal plumes at the Brothers submarine volcano, Kermadec arc, New Zealand. *Economic Geology*, *118*(7), 1549–1561. https://doi.org/10.5382/econgeo.4998

Walker, S. L., de Ronde, C. E. J., Fornari, D., Tivey, M. A., & Stucker, V. K. (2016). High-resolution water column survey to identify active sublacustrine hydrothermal discharge zones within Lake Rotomahana, North Island, New Zealand. *Journal of Volcanology and Geothermal Research*, *314*, 142–155. https://doi.org/10.1016/j.jvolgeores.2015.07.037

Watts, A. B., Peirce, C., Grevemeyer, I., Pauletto, M., Stratford, W., Bassett, D., et al. (2012). Rapid rates of growth and collapse of Monowai submarine volcano, Kermadec Arc. *Nature Geoscience*, *5*(7), 510–515. https://doi.org/10.1038/ngeo1473

Williams, M., Mackay, K., Zwolak, K., Sharma, S., Simpson, B., & the TESMaP Project Team. (2022). Mapping the seabed changes from the Hunga Tonga-Hunga Ha'apai eruption. In *Abstract V16A-01 presented at 2022 AGU fall meeting, 12–16 December*.

World Bank. (2022). *The January 15, 2022 Hunga Tonga-Hunga Ha'apai eruption and tsunami, Tonga: Global rapid post disaster damage estimation (GRADE) report* (p. 42). International Bank for Reconstruction and Development / The World Bank.

Wright, I. C., Chadwick, W. W., Jr., de Ronde, C. E. J., Reymond, D., Hyvernaud, O., Gennerich, H.-H., et al. (2008). Collapse and reconstruction of Monowai submarine volcano, Kermadec arc, 1998–2004. *Journal of Geophysical Research*, *113*(B8), B08S03. https://doi.org/10.1029/2007JB005138

Yeo, I. A., McIntosh, I. M., Bryan, S. E., Tani, K., Dunbabin, M., Metz, D., et al. (2022). The 2019–2020 volcanic eruption of Late'iki (Metis Shoal), Tonga. *Scientific Reports*, *12*(1), 7468. https://doi.org/10.1038/s41598-022-11133-8

Yuen, D. A., Scruggs, M. A., Spera, F. J., Zheng, Y., Hu, H., McNutt, S. R., et al. (2022). Under the surface: Pressure-induced planetary scale waves, volcanic lightning, and gaseous clouds caused by the submarine eruption of Hunga Tonga-Hunga Ha'apai volcano. *Earthquake Research Advances*, *2*(3), 100134. https://doi.org/10.1016/j.eqrea.2022.100134

Zhu, Y., Bardeen, C. G., Tilmes, S., Mills, M. J., Wang, X., Harvey, V. L., et al. (2022). Perturbations in stratospheric aerosol evolution due to the water-rich plume of the 2022 Hunga-Tonga eruption. *Communications Earth & Environment*, *3*(1), 248. https://doi.org/10.1038/s43247-022-00580-w